Latin American Journal of Solids and Structures
www.lajss.org

Dynamic Response and Microstructure Evolution of Oxygen-Free High-Conductivity Copper Liner in Explosively Formed Projectile

Abstract

The dynamic response and microstructure evolution of oxygen-free high-conductivity copper in a shaped charge liner are investigated through microstructural examination of a soft-recovery EFP. Adiabatic shear bands and voids which is the failure original of copper EFP can be observed in the rear part of the projectile. Numerical simulation results illustrate that the highest plastic strain reaches about 2.9 which can fully accommodate the grains deformation of copper EFP during the formation process at strain rates of the order of $10^4 s^{-1}$. Theoretical calculation results indicate that the highest temperature increase of EFP caused by shock wave and plastic deformation can reach $747K$, which is $0.55T_m$ (where T_m is the melting temperature of copper). The main body of the EFP undergoes completely dynamic recrystallisation, and the average size of the refined grains significantly decreases to approximately 10μm. A slight increase in grain size occurs mainly away from the center and extends towards the head and rear sections of the EFP. During the DRX process, the dislocation movement is believed to be the controlling mechanism significantly refining the microstructure.

Keywords

Explosively formed projectile; Plastic strain; Temperature rise; Microstructure evolution; Dynamic recrystallisation

JianFeng Liu [a]
Yuan Long [a, *]
Chong Ji [a]
Daofeng Xu [b]
Dong Xiang [c]
Ge Song [a]

[a] College of Field Engineering, PLA Univ. of Sci. & Tech., China
[b] Hubei Weidong Chemisthy Industries Limited Liability Company, China
[c] The First Engineers Scientific Research Institute of the General Armaments Department, China

* Corresponding Author Email: long_yuan@sohu.com

http://dx.doi.org/10.1590/1679-78253958

Received 23.04.2017
In revised form 30.07.2017
Accepted 05.08.2017
Available online 26.08.2017

1 INTRODUCTION

Explosively formed projectile(EFP) is a kind of shaped charge structure which exhibits high penetration ability in the field of weapon engineering [Yu et al.,1999; Weickert et al.,1993]. A complete EFP warhead consists of a metallic liner, high-energy explosive (HE), case, a slotted ring or sleeve

and a detonator. After detonation, the dynamic interactions among the explosive products, case and liner present a challenging problem for designers to optimize EFP warhead [Wu et al.,2007]. Johnson [1981,2006] firstly demonstrates the influence of geometrical parameters, including shell (liner) thickness, eccentric initiation and asymmetries in a shaped charge on the formation parameters of EFP. Similar studies are extensively conducted by Bender et al. [1993,1994], Weimann [1990] and Weickert et al. [1996]. Their studies focus on the aspect ratio (length-to-diameter ratio) of the explosive, case and liner. Recently, Li et al. [2010] examine the effects of the position, timing and number of detonation points on the EFP formation. They conclude that the velocity and penetration capability of projectile increase when the number of detonation points increases. Cardoso and Teixeira-Dias [2016] evaluate and assess the performance of EFPs with different configurations, materials and detonation conditions. Among the materials and within the range of the parameters tested, the most aggressive EFP presents a copper liner with thickness of 4%–7% of its diameter and HE. Besides, many other investigators have studied the effects of different factors on the performance parameters of EFP, and their efforts have considerably improved terminal effects of warhead over the years. And these researches on the EFP formation process and improvement of terminal effects may have reached its limit at the macroscopic analysis level. However, the formation and penetration process of EFP remains incompletely understood, and several basic issues need to be further investigated, especially the mechanism on the microstructural evolution of the liner under extreme conditions including high pressure and temperature[Meyers,1994]. A detailed and systematic study on EFP formation process is necessary to gain fundamental insights into its microstructural level.

As a key component of EFP warhead, the liner undergoes extreme yet controlled plastic deformation induced by an explosive. During the formation process, an EFP liner experiences essentially plastic strains up to 300%, at strain rates of the order of 10^4 s^{-1}. Tantalum, copper, iron, molybdenum and tantalum-tungsten alloys have been used in EFP warhead. A detailed microstructural analysis on Ta EFPs by Murr et al. [1996,1997] reveals that dynamic recovery (DRV) is a predominant mechanism influencing the EFP formation. They use several analytical tools and microanalysis approaches to identify and resolve the microstructural and microchemical issues in material. Pappu et al. [2000] observe dense Neumann bands in the central region of the head of an iron EFP and provide transmission electron microscopy(TEM) evidence indicating that they are indeed deformation twins. Therefore, the properties of the liner are important in the context of the dynamic EFP formation process. The eventual effectiveness of the liner as a penetrator is attributed to its high density, high ductility, high strength and sufficiently high melting temperature which prevents melting caused by adiabatic heating. The Oxygen-free High-conductivity(OFHC)copper shows a good combination of these properties and is also one of the most commonly preferred material. Nevertheless, the literature review clearly reveals the microstructural evolution of OFHC copper liner driven by HE is limited and inconsistent.

In the current study, a “soft-catch” device is designed for the safe recovery of EFP. Optical metallography, scanning electron microscopy(SEM) and TEM techniques are used to provide a detailed overview of the EFP microstructures. Combined with simulation and theoretical calculation results, we analyse the microstructure evolution, including dynamic recrystallisation and refined grains, in the typical zones of the EFP.

2 EXPERIMENTAL PROCEDURE AND RESULTS

In order to obtain an original stable form of EFP, a soft-recovery device that can safely decelerate and recover the intact projectile for the characterization of its material properties at its end state is designed. The mathematical model is based on the observations presented by Allen et al. [1957]. The initial application of this model to a specific EFP design shows promising results[Pope et al.,2005; Lambert et al.,2005]. In our experiment, an EFP warhead is installed in front of the soft-recovery device, and the standoff allows a flight distance of over 5m, ensuring full formation (complete at nominally 0.5m) of EFP. A square channel pipe with length of 13 m, cross section of 0.36 m, and wall thickness of 0.04m is used. Various soft-catch media are full of the square channel pipe. The media are composed of expanded polystyrene (50,150,300 and 500kg/m^{3,} separately), water (993 kg/m^3) and sand from their entrance onward. Before a stable formation projectile exists in the soft-recovery apparatus, an X-ray machine is used to obtain the length, diameter, head velocity and trail velocity of the projectile. These parameters are essential to characterise the media by using the soft-recovery model. The schematic structure of the soft-recovery apparatus is shown in Figure 1.

The EFP is obtained from a dish-shaped OFHC copper liner backed by 8701 HE. The 8701 HE with a nominal density of 1.71 g/cm^3 and a detonation velocity of 8315 m/s is initiated by a pressed PBX 9407 explosive precision booster and an 8# detonator. The chemical compositions of the explosive and copper liner are summarised in Table 1.

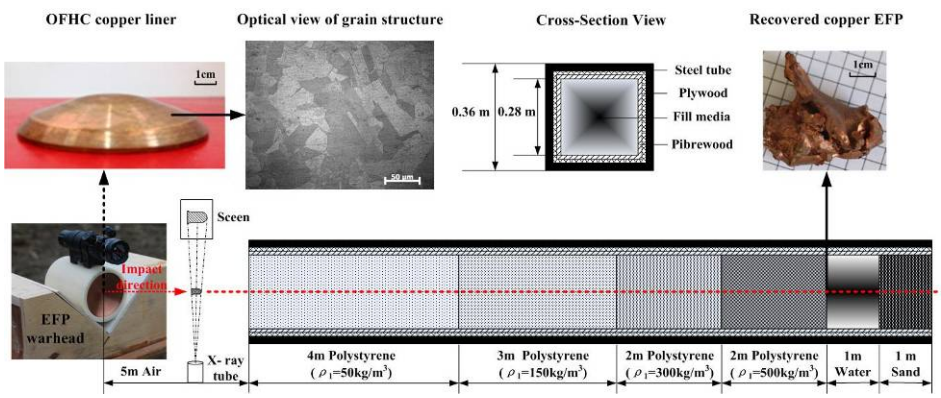

Figure 1: Experimental setup of soft-recovery apparatus.

8701 HE	Hexogen 94.5		Polyvinyl acetate 2.0		Dinitrotoluene 3.0		Stearic acid 0.5	
Copper	Zn	Sn	Sb	Pb	Ni	S	Fe	Cu
	0.0018	0.0015	0.0018	0.003	0.0015	0.003	0.003	Balance

Table 1: Chemical compositions of 8701 HE and copper liner (wt.%).

After the soft-recovery process in the impact test, the recovered complete copper EFP is cut by a wire electrical discharge machine. Figure 2 shows the longitudinally sliced half sections of the soft-recovered EFP. Due to the interaction between the copper EFP and soft media in the recovery device, there is a slight fracture in the rear regions of the copper EFP where the material is prone

to failure, such as EFP head, EFP rear and EFP fins. A multi-layer structure filling soft media with increasing densities is used in the experiment to weaken this effects on the microstructural features of the EFP. Therefore, the metallographic results of the copper EFP in our experiment can be ideally dealt with the microstructures of copper liner driven by explosive ignored other minor influences during the formation and soft-recovery process.

Figure 2: Longitudinally sliced half sections of soft-recovery EFP. (s) EFP surface, (a) EFP head, (b) EFP center, (c) EFP rear and (d) EFP fin.

In the experiment, a large number of laminar flow ripples spread evenly on the surface of EFP, as displayed in Figure 2(s). When the surface of the soft-recovery EFP is electro-polished and examined by SEM, a considerable number of laminar flow ripples similar to those previously reported by Tao et al. [2008] are observed. Further observations reveal that these ripples distribute layer by layer and are the prominent microstructural features of the EFP surface. The enlarged view exhibits details of these ripples which behave more like a kind of liquid driven by HE. The appearance of the ripples can be attributed to the coupling effects of the shock wave and severe plastic deformation of liner. The typical regions (head, center, rear and fins) of the EFP are also been carried on microstructural observation along the longitudinally sliced half section, as shown in Figure 2 (a, b, c and d).

3 NUMERICAL STUDY ON THE FORMATION PROCESS OF EFP

3.1 Establishment of the Simulation Model

Numerical simulation is carried out using three-dimensional (3D) dynamic finite element program of LS-DYNA in order to study the formation of EFP. The simulation model of the EFP warhead is presented in Figure 3. Due to symmetry, modelling 1/2 of the geometry is necessary to simplify the analysis and reduce the computational cost.

The explosive and liner are meshed by Lagrangian algorithm with hourglass control. In order to improve the quality of the discrete elements, numerical model is discretized with 8-node hexahedral solid elements(SOLID164). [Hallquist, 1997; Cardoso et al., 2016] For a circular liner in an axisymmetric EFP warhead, Figure 3 shows the gridding results considered in our study. This approach provides elements that are approximately equally sized, but some asymmetries are introduced and

some elements are not formed in a compact manner. In an effort to introduce more symmetry into the grid, it is possible to put uniform rings around the outer portions of the circle, as shown in the meshing process of liner. This provides the same number of elements in each of the uniform rings. Here the asymmetries are reduced, but the elements get larger and larger as they move outward (for a constant radial increment), as shown in Figure 3. [Hallquist, 1997; Johnson et al., 2006] *BOUNDARY_SPC_SET [Hallquist, 1997] is used in the simulation model to restrict elements movement in the symmetrical boundaries. *CONTACT_SLIDING_ONLY_PENALTY [Hallquist, 1997] is used to model the impact between the dynamite and liner. A large number of numerical calculation results can prove that detonation products at about 30 μs will no longer affect the characteristic parameters of EFP after the explosive is detonated. Therefore, the explosive is deleted at 30 μs in the numerical calculation [Liu et al., 2017].

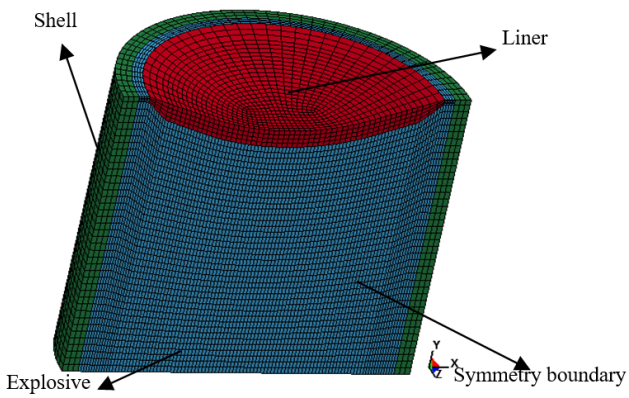

Figure 3: Simulation model of EFP warhead (1/2 model).

3.2 Material Constitutive Models and Parameters

3.2.1 Material Model for High Explosive

HE is typically modeled by using the Jones-Wilkins-Lee (*JWL*) EOS, which models the pressure generated by chemical energy in an explosion. It can be written in the form

$$p = A_1\left(1-\frac{\omega}{R_1 v}\right)e^{-R_1 v} + B_1\left(1-\frac{\omega}{R_2 v}\right)e^{-R_2 v} + \frac{\omega e}{v} \tag{1}$$

where p is the hydrostatic pressure, v is the specific volume, e is internal specific energy. The values of constants A_1, R_1, B_2, R_2 and ω for many common explosives have been determined from dynamic experiments.

3.2.2 Material Model for Liner

To be able to describe the various phenomena taking place during contact explosion, it is necessary to characterize the behavior of material under explosion-generated high strain rate loading condition. Liner is modeled by the Johnson-Cook (*J-C*) material model [Johnson and Cook, 1983], which is

suitable to model the strength behavior of materials subjected to large strains, high strain rates and high temperatures. The model defines the yield stress σ as

$$\sigma = \left(\sigma_0 + B\varepsilon^n\right)\left(1 + C\ln\frac{\dot{\varepsilon}}{\dot{\varepsilon}_0}\right)\left(1 - T^{*n}\right) \tag{2}$$

where A, B, C, n and m are the material parameters determined by experiments. $\bar{\varepsilon}^p$ is the equivalent plastic strain, $\dot{\varepsilon}^* = \dot{\varepsilon}_p / \dot{\varepsilon}_0$ is the dimensionless effective strain rate at a reference strain rate $\dot{\varepsilon}_0 = 1\,s^{-1}$. T^* is the homologous temperature which is defined by $T^* = \left(T - T_{\text{room}}\right)/\left(T_{\text{melt}} - T_{\text{room}}\right)$, where T is the current temperature, T_{room} and T_{melt} are the room and melting temperatures, respectively.

Johnson and Cook [1985] also developed a failure criterion that accounts for temperature, strain rate and strain path in addition to the triaxiality of the stress state. The model is based on damage accumulation, and has the basic form

$$D = \sum \frac{\Delta\varepsilon}{\varepsilon_f} \tag{3}$$

where D is the damage to a material element, $\Delta\varepsilon$ is the increment of accumulated plastic strain, and ε_f is the accumulated plastic strain to failure under the current conditions of stress triaxiality, strain rate and temperature. Failure occurs when D=1, and in the finite element simulations, element erosion is used to remove elements that have reached the critical damage. The failure strain ε_f is defined as

$$\varepsilon_{\text{f}} = [D_1 + D_2 \exp D_3\sigma^*][1 + D_4 \ln\dot{\varepsilon}^*][1 + D_5 T^*] \tag{4}$$

where σ^* is the dimensionless pressure-stress ratio defined as $\sigma^* = \sigma_{\text{m}}/\bar{\sigma}$, where σ_{m} is the mean stress normalized by the effective stress, $\bar{\sigma}$ is the effective stress, and D_1, D_2, D_3, D_4 and D_5 are the material parameters [Johnson and Cook, 1985]. Details of finite element modeling of 8701 explosive and copper liner are described in Table 2 [Liu et al., 2017].

8701 explosive	ϱ (g/cm^3)	D (km/s)	P_{CJ} (GPa)	A_1 (GPa)	B_1 (GPa)	R_1	R_2	ω	E_0 (GPa)	V_0
	1.71	8.315	28.6	524.23	7.678	4.20	1.1	0.34	8.499	1.00
Copper	ϱ (g/cm^3)	G (GPa)	A(MPa)	B(MPa)	N	C	m	T_{m}	σ_{s} (GPa)	C (km/s)
	8.97	46.50	90	292	0.31	0.025	1.09	1356	0.09	3.94
	S_1	S_2	S_3	γ_0	a	E_0	V_0			
	1.49	0	0	2.02	0.47	0	1.0			
	D_1	D_2	D_3	D_4	D_5					
	0.54	4.89	-3.03	0.014	1.12					

Table 2: Parameters of 8701 HE and copper.

3.3 Dynamic Response of Copper Liner in EFP Warhead

According to the detonation waveform theory [Ye, 2003], when the top center of the cylinder charge explodes, the detonation wave is a spherical wave. A high-pressure shock wave propagates through the explosive and interacts with the liner, which is accelerated while simultaneously being reshaped into a rod of desired shape. The sequence of transforming a copper liner into a slug is schematically shown in Figure 4. Selecting typical elements at different liner positions, as shown in Figure 4(e): (1) EFP head, (2) EFP center, (3) EFP rear and (4) EFP fin. The central portion of the liner moves relatively fast and developed into a 'head' section, whereas the other parts of the liner, travelling at relatively low speeds, lagged behind and formed the rear section of the slug. As the appearance of EFP is stable, the velocity of the EFP is 1503m/s, and the dimensionless ratio value of the length and diameter is approximately 2.6 according to simulation results. In the experiment, the velocity of the EFP is 1495m/s. The results of simulation are in good agreement with the experimental results and it also shows the reasonable of selected numerical models and accuracy of material parameters.

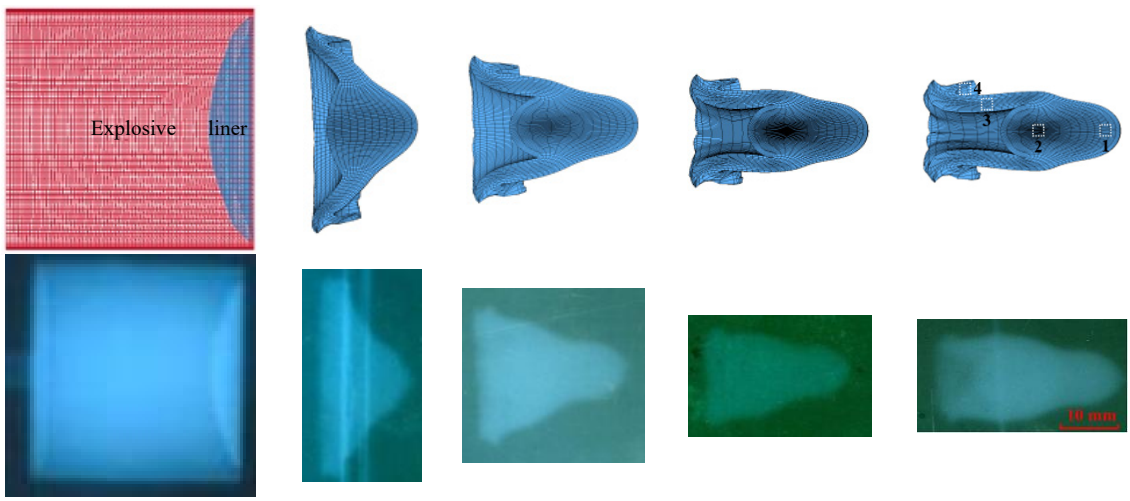

(a) t =0 us (b) t =35 us (c) t =60 us (d) t =80 us (e) t =160 us

Figure 4: Formation process of EFP (Simulation results and X-ray images).

In the longitudinally sliced half section of soft-recovery EFP, two typical kinds of plastic deformations of liner have been observed, the adiabatic shear deformation along the movement direction of the EFP under the action of the shock wave and deformation caused by radial shrinkage of the liner during the collapse process towards the axial direction of the liner. The microscopic characteristics of these plastic deformations can be observed mainly in the rear sections of EFP, as presented in Figure 5(a, c and d). The material in the rear part of the EFP is elongated along the movement direction of EFP and micro-cracks are evenly distributed on this zone because of severe plastic deformation. In the central zone of EFP, the microstructure is more uniformly refined because of the symmetrical external force acting on this part material during the formation process of the EFP, as shown in Figure 5(b).

According to the optical microscopy results, adiabatic shear bands are observed mainly in the rear regions of the EFP where these parts of the material is prone to failure in the mode of fracture in the experiment, such as EFP head, EFP rear and EFP fins, as shown in Figure 5. In facts, the deformed and fractured behaviour generates mainly along the region of EFP head and EFP fins in our soft-recovery test. The shear bands run almost perpendicular to the longitudinal axis, extending through the EFP fins and causing premature failure of the projectile. Observing the morphology surfaces of EFP fins, voids and parabolic dimples are distributed on the fracture surfaces indicating the EFP fins experience severe plastic deformation during the formation process, as shown in Figure 6. In this mode of failure, the material of EFP fins fails due to ductile fracture caused by overstretching along radial of EFP during the formation process.

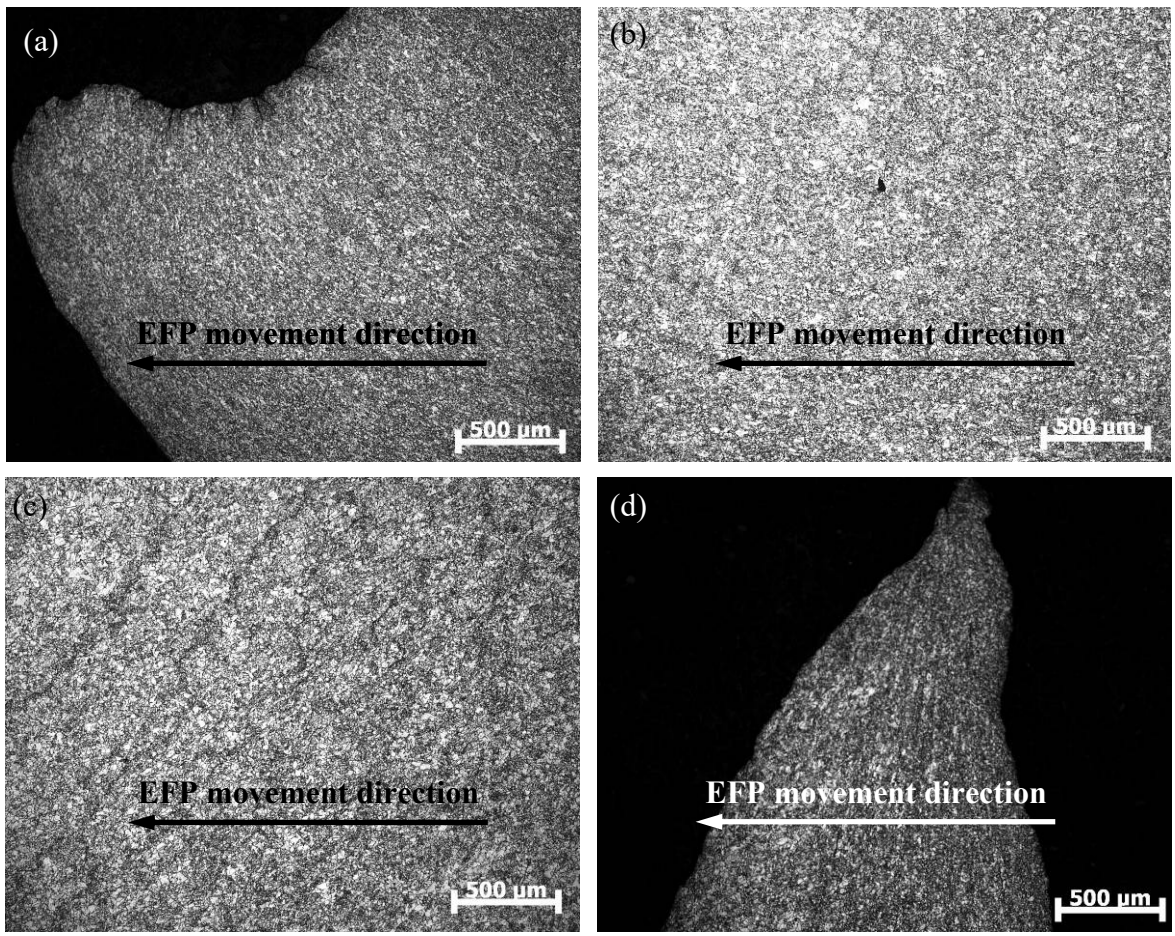

Figure 5: Optical metallographic images of microstructural characteristics of the typical zones of copper EFP correspondingly in Figure 2. (a) EFP head, (b) EFP center, (c) EFP rear and (d) EFP fin.

Corresponding numerical simulation results indicate that different regions of the EFP undergo various degrees of plastic deformation. The greatest plastic strain in the EFP center can reach as high as 2.9 along the longitudinal axis of EFP, as shown in Figure 7. And the effective strain begins to drop rapidly as the position away from the EFP center. Considering the formation process of

EFP and extremely plastic deformation in the main body of copper EFP, the high plastic strain can fully accommodate the grains deformation of copper liner during these dynamic process. The maximum rate of plastic strain can reach as high as 1.8 x 10^4 s^{-1} since the formation process of EFP can be completed in 160μs as shown in Figure 4.

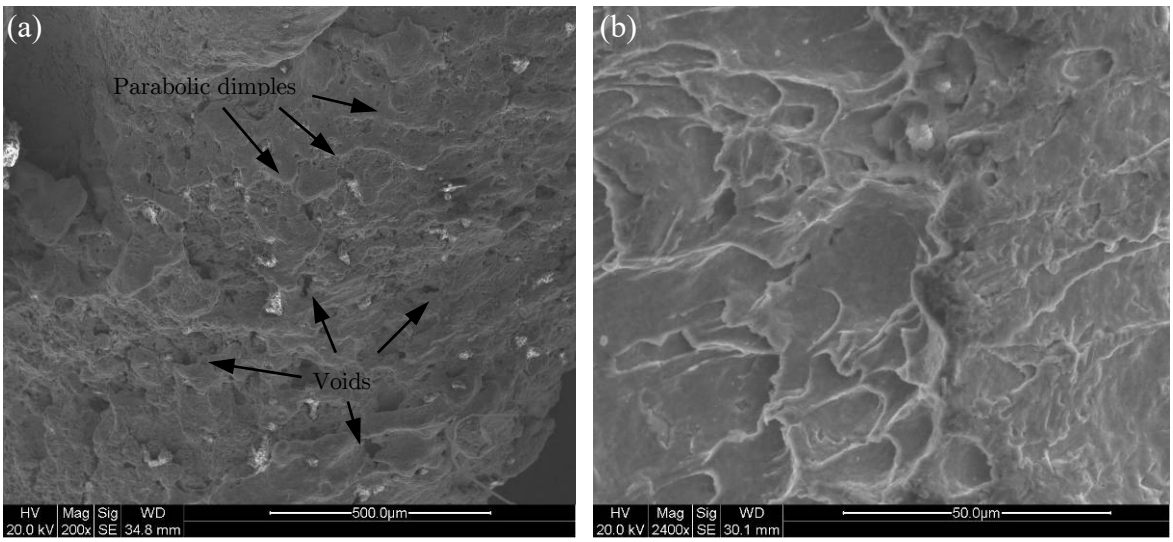

Figure 6: Morphology features of fracture surfaces of EFP fins. (a)Fracture surfaces, (b)Parabolic dimples.

However, the hydrocode cannot consider the influence of shear localization and is therefore incapable of predicting the local premature fragmentation of the projectile. The present study indicates that one reason for the flow localization is deformation-heating-induced softening since the formation of shear bands is found to be associated with a critical strain. This is in agreement with a thermal instability model which is originally formalized by Culver [1973] and modified later by Semiatin and Jonas [1984]. This model yields a simple equation relating the critical shear strain γ_i for the onset of localization during high strain rate deformation to other experimentally determined material parameters:

$$\gamma_i = \frac{\rho c_P n}{\beta(\partial\tau/\partial T)_{\gamma,\dot{\gamma}}} \tag{5}$$

where ϱ is the density, c_P is the specific heat, n is the work-hardening exponent, τ is the shear flow stress, T is the temperature, γ is the shear strain, $\dot{\gamma}$ is the shear strain rate and β is the fraction of plastic work converted to heat. For OFHC copper, c_P=385J/(kg K), β=0.9 and $\partial\tau/\partial T$ is estimated to be 0.45 MPaK^{-1} [Tang et al., 1991]. Substituting data into Eq.(5)，one finds that γ_i=2.6. The critical strain for initiation of macroscopic shear bands in copper during rolling is reported to be 2.5-3 [Hatherly et al., 1984]. This indicates that Eq.(5) gives a good estimate. Optical metallography performed on the projectile confirms that the region where many adiabatic shear bands developed also experiences, according to the hydrocode modeling, a strain in excess of 2.6, as shown in Figure 7.

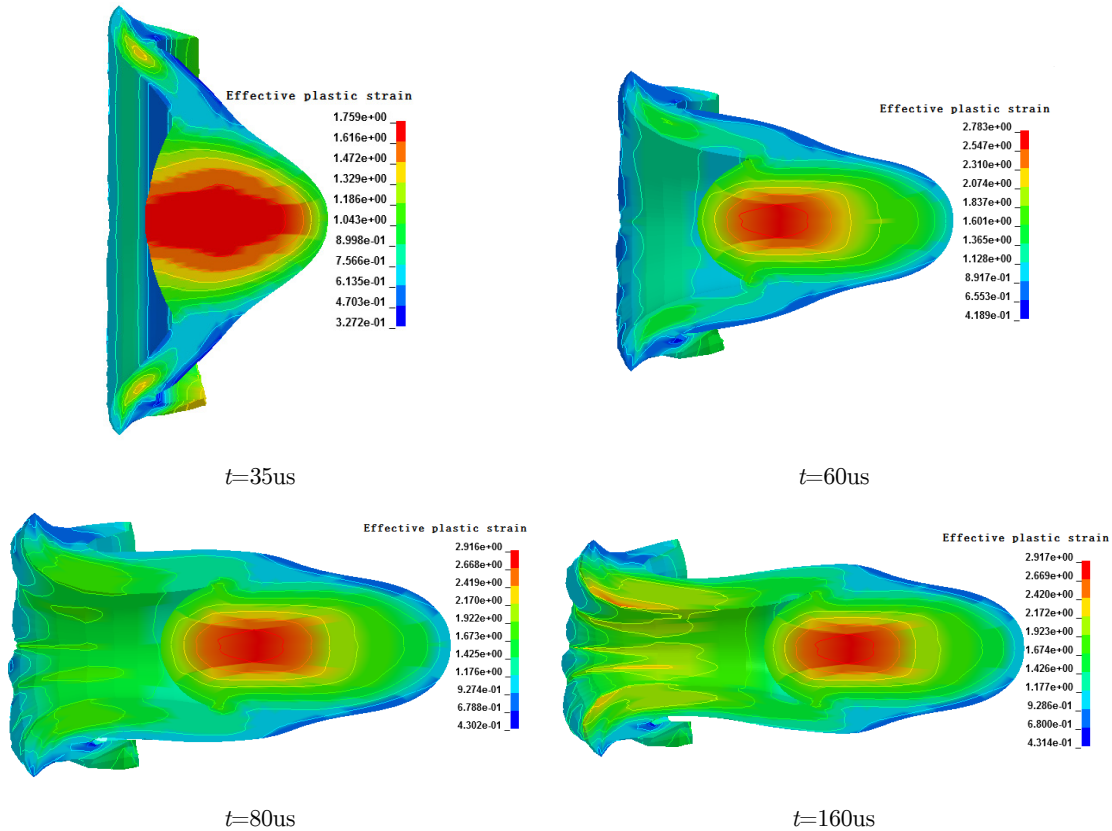

Figure 7: Effective plastic strain of EFP.

Close examination of Figure 6(a) reveals that a large number of voids existed in the copper EFP fins, especially at the rear position of the fracture surfaces. Since the parabolic dimples are not yet fully developed, one may conclude that, in this case, void formation does reduce the load-bearing capacity of the region, thus leading to the material failure of rear part of EFP. In fact, the distribution of voids takes an advantage in the areas of EFP head, EFP rear and EFP fins, typical features of voids are shown in Figure 8. It is known that the critical strain at which the shear bands develop is very sensitive to in-homogeneities [Tvergaard et al., 1982], and void nucleation at the in-homogeneities can promote plastic flow localization and shear instability [Saje et al., 1982]. A simple view is that the macroscopic effect of void formation causes an apparent volume loss of load-bearing material. The shear bands observed in the rear position of projectile are most likely triggered by void formation [Argon et al., 1975].

The structure change of solid is governed by external factors such as pressure and temperature and internal factors such as composition and internal stresses due to defects (dislocations, point defects, interface)[Antoun.,2003]. High velocity impact caused by detonation wave of explosive produces sudden changes of pressure that may result in polymorphic transformations and microstructural evolutions of the copper liner [Murr et al., 2002; 2004]. Figure 9 illustrates pressure versus time plots at different regions of copper liner. Although the initial shock wave acting on the liner may be considered to be approximately planar, the interaction style between detonation wave and

liner gradually changes from the incident to oblique penetration. As a result, the pressure value of detonation wave acting on the liner gradually reduces from the central position to the edge portion of the liner. Therefore, the liner experiences a very complex pressure loading process during deformation process of EFP. Regions 1 through 4 experience maximum pressures of 12.68GPa, 26.25GPa, 20.10GPa and 9.37GPa, respectively.

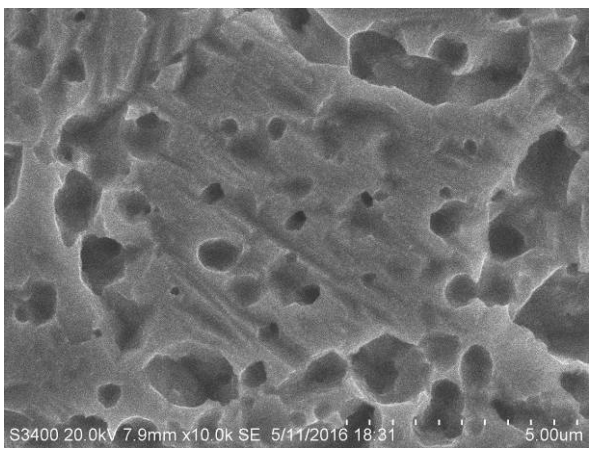

Figure 8: Voids distributed in the rear regions of the EFP.

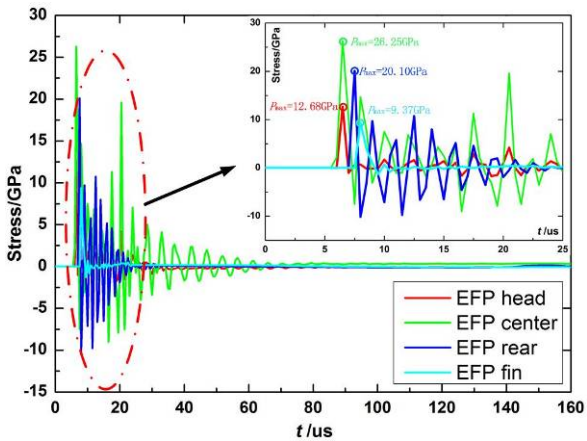

Figure 9: Pressure versus time plots at different regions of liner.

4 MICROSTRUCTURE EVOLUTION OF OXYGEN-FREE HIGH-CONDUCTIVITY COPPER LINER

4.1 Temperature Increase Caused by Shock Waves and Plastic Deformations

Once initiation, a high-pressure shock wave with peak pressure of approximately 30GPa propagates through the explosive and interacts with a 3.5mm thick liner. The absolute time of the interaction between the shock wave and each liner element is less than 0.5μs [Zhang et al., 2012]. The collapse velocity caused by the shock wave at different times varies from the top to the bottom of the liner. The liner experiences severe shear deformation movement caused by the different interaction sequences between the shock wave and liner elements. The copper liner exhibits temperature variation caused by shock waves and severe plastic deformation driven by HE explosion load. Approximately 10 μs to 30μs is observed in the interaction between the shock wave and the liner before the stable formation of EFP [Liu, 2014]. The extremely short duration of the EFP formation process precludes any experimental observation of the microstructural evolution and temperature change during this process. The temperature change caused by shock waves T_s and plastic deformations T_r in the liner is an important criterion for the analysis of the thermal effects and microstructural evolutions of the liner and can be calculated as follows.

Shock waves compress the liner, thus increasing the temperature of the latter. The thermodynamic process at the shock front is assumed to be adiabatic. The release from shock state to initial state is usually assumed to be isentropic. The shock temperature T_s can be calculated by [Cao et al., 2005]

$$T_s = T_0 \exp\left[\frac{\gamma_0}{v_0}(v_0 - v_1)\right] + \frac{p(v_0 - v_1)}{2c_v} + \frac{\exp\left(\frac{r_0}{v_0}v_1\right)}{2c_v}\int_{v_0}^{v_1} p\exp\left(\frac{r_0}{v_0}v\right)\left[2 - \frac{r_0}{v_0}(v_0 - v)\right]dv \tag{6}$$

where γ_0 is the Mie-Gruneisen state parameter of copper and γ_0=1.99. P is the peak pressure of the shock wave and v_0 is the initial specific volume of material. v_1 is the specific volume of the material directly behind the shock and this volume can be calculated from the relationships among the shock parameters

$$v_1 = \frac{c_0^2}{2pS^2}\left[\sqrt{1 + \frac{4pSv_0}{c_0^2}} + \frac{2S(S-1)v_0 p}{c_0^2} - 1\right] \tag{7}$$

where c_0 and S are the parameters used to describe the relationship between shock velocity U_S and particle velocity U_P

$$U = c_0 + S_1 U_P \tag{8}$$

For the copper material, c_0=3.94km/s and S_1=1.49km/s. The heat capacity c_v (specific heat at constant volume) is also considered. The values of the specific heat at constant pressure c_v can be expressed by Eq.(9)

$$c_v = T(\partial S/\partial T)_V \tag{9}$$

The residual temperature of EFP T_R can be viewed as an isentropic release process and can be expressed by

$$T_R = T_s \exp\left[\gamma_0(v_1 - v_0)/v_0\right] \tag{10}$$

Both T_S and T_R increase when the peak pressure of the shock wave increases, as shown in Figure 10. The residual temperature of EFP T_R is about 367K when the intensity of shock wave reaches 30GPa. This result indicates that the temperature of EFP increases by 97K as the initial temperature T_0 of EFP is 270K.

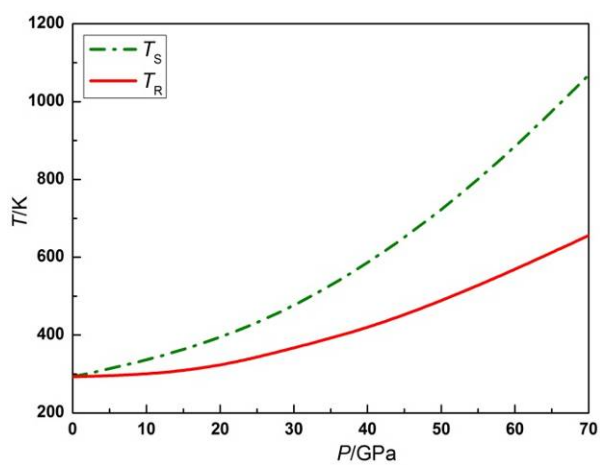

Figure 10: Temperature increase caused by shock wave.

The temperature increase associated with plastic deformation can further calculated from the constitutive responses of the copper based on the temperature increase caused by shock waves. Indeed, the temperature increase caused by plastic deformation can be expressed as [Meyers, 1994]

$$\Delta T = \frac{\beta}{\rho c_p}\int_0^{\varepsilon} \sigma d\varepsilon \tag{11}$$

The strength of the material σ is described by the Johnson–Cook model, as shown in Eq.(2). The temperature change due to the plastic deformation can be expressed as

$$\Delta T = \left[1-\exp\left(\frac{-\beta\left(1+C\log\dfrac{\dot{\varepsilon}}{\dot{\varepsilon}_0}\right)}{\rho c_p\left(T_m-T_r\right)}\times\left(\sigma_0\varepsilon+\frac{B\varepsilon^{n+1}}{n+1}\right)\right)\right]\left(T_m-T_r\right) \tag{12}$$

where T_r=367K, T_m=1356 K, B=53.7MPa, C=0.026, σ_0=330MPa (the value for shock-hardened steel target), m=1.04, ϱ=9.05 g/cm^3 and $\dot{\varepsilon}=1s^{-1}$ [Cao et al., 2005].

Figure 11 demonstrates the increase of temperature as a function of the strain caused by plastic deformation. Generally, the temperature increase caused by severe plastic deformation is less than 400K (the current temperature of EFP is 747K) when the plastic strain of the copper liner is less than 3. A considerable amount of local heat is generated around the severe plastic deformation zone, the temperature is still far from the melting point of OFHC copper(1356K). The EFP which collapses from the liner is usually considered as a 'fluid' metal projectile. However, this feature does not indicate that the liner temperature reaches the melting point of the liner when it undergoes shock loads of HE.

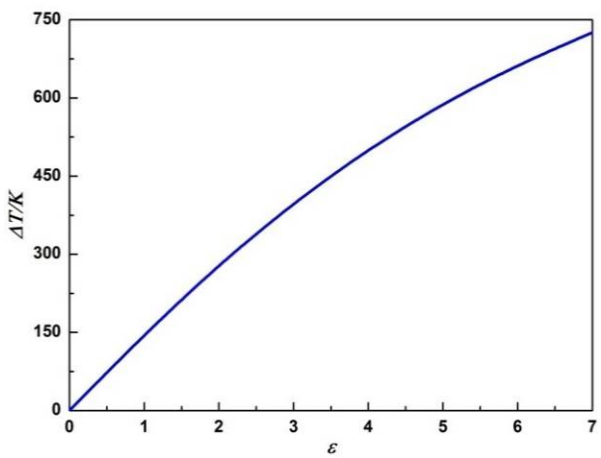

Figure 11: Temperature increase associated with plastic deformation.

Although the microstructural behaviour of the liner material nearly exhibits a liquid state under high pressure and temperature conditions, no evidence of melting or melt-related (solidification) microstructures in the body of the EFP has been found. The stretched fluid appearance of the EFP probably occurs because the liner is hot deformed into a projectile with a diameter of not more than 0.3 times that of the initial liner. With such extremely high strain rate and transient load relative to the ordinary pressure bar test and strain measurement, severe plastic deformation of the copper liner can be expected to occur primarily through the extreme plastic flow, which is a potential superplastic flow in solid state [Chokshi et al., 1990].

4.2 Microstructural Evolution of the Copper Liner

Representative optical micrographs in the typical positions of copper EFP are shown in Figure 12. The microstructures of the completely recrystallised grains, micro-cracks and twins appear on the EFP half section. The initial EFP liner grain size of roughly 63.12 μm has been refined, as shown in Figure 1 and Figure 12.

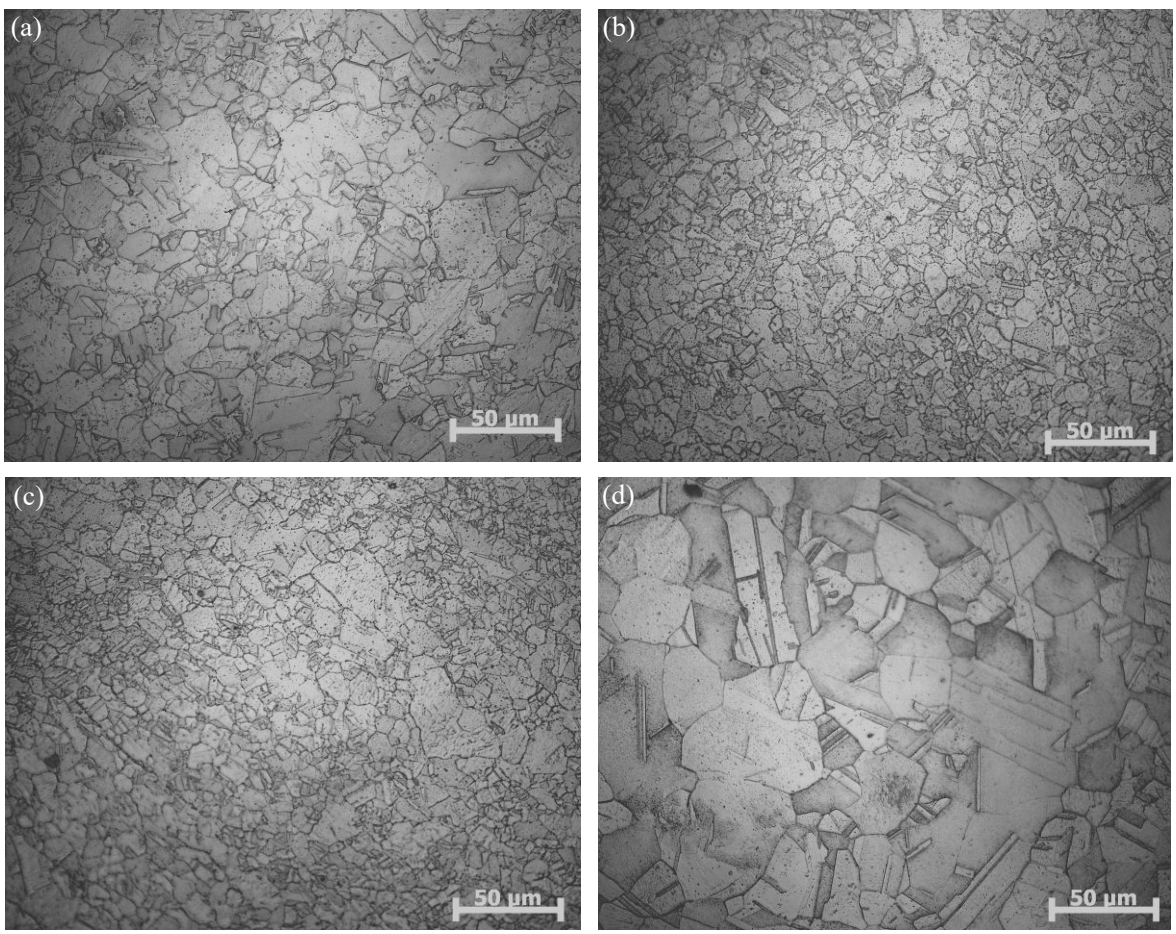

Figure 12: Optical micrographs of longitudinally sliced half section of the copper EFP microstructures. Numbers (a)-(d) correspond to the half-section locations in (a)-(d) shown in Figure 2.

On the average, the grain sizes of EFP head, center, rear and fins are 19.85, 9.12, 13.74 and 42.70μm, respectively. The grain sizes are obtained by calculating the average size of hundreds of grains in more than five micrographs of each of the four sections (EFP head, center, rear and fins). The main body of the EFP experiences severe plastic deformations and temperature variations and it is mainly composed of a series of DRX grains with some variations in the grain sizes. A slight increase in grain size occurs mainly away from the center and extends towards the head and rear sections of the EFP, as shown in Figure 12(a-c). This finding indicates that a complete recrystallisation process occurs in these zones. The highest temperature in the EFP can reach 747 K. Thus, an intermixing of static and dynamic recrystallisation (grain growth indicates post-deformation temperature effects) [Pappu, 2000] may have possibly occurred because the material of copper exhibits a fairly low minimum recrystallisation temperature of 473 K, which is $0.35T_{\mathrm{m}}(\mathrm{K})$ (where T_{m} is the melting temperature of copper) [Brick et al., 1977]. The microstructure evolution of copper EFP has a good agreement with theoretical calculation result under high velocity impact.

During the dynamic process of recrystallisation in the main body of copper EFP, plastic deformation by dislocation is the predominant mechanism that governs DRX process. Figure 13 provides evidence that dislocation gliding facilitates grain refinement in the DRX process. Figure 13(a) shows TEM image of DRX grains in the centre of EFP and Figure 13(b) shows a corresponding selected-area electron diffraction(SAED) pattern of microstructures.

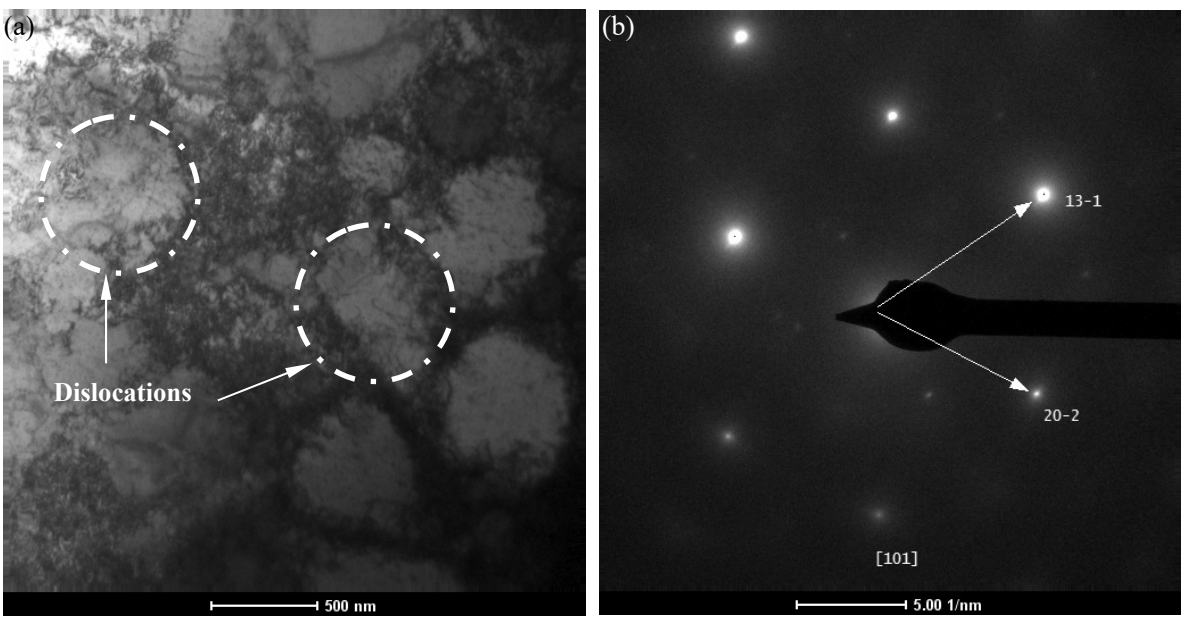

Figure 13: TEM image of DRX grains in the center of EFP and selected-area electron diffraction(SAED) pattern of microstructures. (a) TEM bright-field(BF) image, (b) SAED pattern in (a).

The presence of dynamically recrystallised grains and dislocation cells is indicative of the occurrences of DRX and DRV. The dislocation substructures generated by shock loading depending on a number of shock wave parameters and the pressure is also the most important one. The 8701 HE in

the EFP warhead generates a compressive shock wave pressure on the copper plate along the axis of roughly 30GPa and the liner experienced a severe plastic deformation with high strain rates over 10^4 s^{-1}. In this condition, increased dislocation density is a warranty for severe plastic deformation, and the dislocation drag controlled plasticity is the only possible mechanism. In the main body of EFP, the matrix grains start fragmenting, recombination and growing under high shock wave pressure and the dislocation mechanism plays a key role in this dynamic process. These fragmented parts eventually form small, recrystallized grains, which help in the further flow of the material [Guo et al., 2009].

5 CONCLUSIONS

In this work, the dynamic response and microstructure evolution of the OFHC copper in a shaped charge liner are investigated in detail on the basis of the analysis of a complete soft-recovery EFP. The major conclusions are as follows:

(1) Adiabatic shear bands and voids which is the failure original of copper EFP can be observed in the rear part of the projectile. Numerical simulation results illustrate that the highest plastic strain reaches about 2.9 which can fully accommodate the grains deformation of copper EFP during the formation process at strain rates of the order of $10^4 s^{-1}$.

(2) Theoretical calculation results indicate that the highest temperature of EFP caused by shock wave and plastic deformation can reach 747K, which is $0.55\,T_m$ (where T_m is the melting temperature of copper).

(3) The main body of the EFP undergoes completely dynamic recrystallisation, and the average size of the refined grains significantly decreases to approximately 10μm. A slight increase in grain size occurs mainly away from the center and extends towards the head and rear sections of the EFP.

(4) The formation process of copper EFP is primarily caused by extreme plastic flow, which is possibly a type of superplastic flow in a solid state. During this large strains, high strain rates and high temperatures process, the dislocation movements are believed to be the controlling mechanisms significantly refining the microstructure and helping in the further flow of the material.

Acknowledgments

The work presented in this paper has been funded by the State Key Laboratory of Explosion Science and Technology under NO. KFJJ10-2M and Advanced Research of PLA University of Science and Technology (201417).

References

Allen W.A., Mayfield E.B. and Harvey H.L., (1957). Dynamics of a Projectile Penetrating Sand. Journal of Applied Physics 28:370-376.

Antoun T., (2003). Spall Fracture, Springer Science & Business Media: New York.

Argon A.S., Im J., and Safoglu R., (1975). Cavity formation from inclusions in ductile fracture. Metallurgical Transactions A, 6(4):825-837.

Bender D. and Carleone J., (1993). Tactical missile warheads. In: Progress in astronautics and aeronautics, American Institute of Aeronautics and Astronautics,155.

Bender D. and Carleone J., (1994). Method and apparatus for providing a explosively formed penetrator having fins. United States Patent, Patent number 5365852,22.

Brick R.M., Pense A.W. and Gordon R.B., (1977). Structure and Properties of Engineering Materials, 4th edn., McGraw-Hill Book Co., NY:83.

Cao B.Y., Lassila D.H., Schneider M.S., et al, (2005). Effect of shock compression method on the defect substructure in momocrystalline copper. Materials Science and Engineering A 409: 270-281.

Cardoso D. and Teixeira-Dias F., (2016). Modelling the formation of explosively formed projectiles(EFP). International Journal of Impact Engineering 93:116-127.

Chokshi A.H. and Meyers M.A., (1990). The prospects for superplasticity at high strain rates: Preliminary considerations and an example. Scripta Metallurgica Materialia 24:605-610.

Culver R.S., (1973). In Metallurgical Effects at High Strain Rates, Eds. R. W. Rohde, B. M. Butcher, J. R. Holland, and C. H. Karnes, Plenum, New York:519-530.

Guo W., Li S.K., Wang F.C., et al, (2009). Dynamic recrystallization of tungsten in a shaped charge liner. Scripta Materialia 60: 329-332.

Hallquist J.O., (1997). LS-DYNA Theoretical Manual, Livermore Software Technology Corporation, Livermore, CA, USA.

Hatherly M.and Malin A.S., (1984). Shear bands in deformed metals. Scripta Metallurgica 18:449-453.

Johnson G.R., (1981). Dynamic analysis of explosive-metal interaction in three dimensions. Journal of Applied Mechanics 48:30-35.

Johnson G.R. and Cook W.H., (1983). A constitutive model and data for metals subjected to large strain, high strain rates and high temperature. In: Proceedings of the 7th International Symposium on Ballistics,Hague,Netherlands:541-548.

Johnson G.R., Cook W.H., (1985). Fracture characteristics of three metals subjected to various strains, strain rates, temperatures and pressures. Engineering Fracture Mechanics 21:31–48.

Johnson G.R. and Stryk R.A., (2006). Some considerations for 3D EFP computations. International Journal of Impact Engineering 32:1621-1634.

Lambert D., Pope M., Jones S., et al, (2005). Soft-recovery of explosive formed penetrators. In: Proceedings of the 22th international symposium on ballistics. Vancouver, BC, Canada: International Ballistics Society: 619-625.

Li W.B., Wang X.M. and Li W.B., (2010). The effect of annular multi-point initiation on the formation and penetration of an explosively formed penetrator. International Journal of Impact Engineering 37:414-424.

Liu J.F., (2014). Study on the formation and penetration properties of Collinear Explosively Formed Projectiles. PhD thesis, Nanjing: PLA University of Science and Technology.

Liu J.F.,Long Y., Ji C., et al,(2017). The influence of liner material on the dynamic response of the finite steel target subjected to high velocity impact by explosively formed projectile. International Journal of Impact Engineering 109:264-275.

Meyers M.A., (1994). Dynamic Behavior of Materials, John Wiley and Sons Inc., New York.

Murr L. E., Pappu S., Kennedy C., et al, (1996). Tantalum Microstructures for High-Strain-Rate Deformation: Shock Loading, Shaped Charges and Explosively Formed Penetrators. In: Tantalum Symposium, TMS Annual Meeting, Anaheim, CA:145-155.

Murr L.E., Meyers M.A., Niou C.S., et al, (1997). Shock-induced deformation twinning in tantalum. Acta Materialia 45:157-175.

Murr L.E., Trillo E.A., Bujanda A.A., and Martinez N.E., (2002). Comparison of residual microstructures associated with impact craters in fcc stainless steel and bcc iron targets: the microtwin versus microband issue. Acta Materialia, 50:121-131.

Murr L.E., and Esquivel E.V., (2004). Review observations of common microstructural issues associated with dynamic deformation phenomena: Twins, microbands, grain size effects, shear bands, and dynamic recrystallization. Journal of Materials Science, 39:1153-1168.

Pappu S., (2000). Hydrocode and microstructural analysis of explosively formed penetrators. PhD thesis, El Paso: The University of Texas.

Pappu S. and Murr L.E., (2000). Shock deformation twinning in an iron explosively formed projectile. Materials Science and Engineering A 284:148-157.

Pope M., Martin B., Lambert D., et al, (2005). Analysis of a Soft Catch for Conventional Warheads. In: the 2005 ASME Pressure Vessels and Piping Division Conference, Denver, Co:17-21.

Saje M, Pan J, Needleman A (1982). Void nucleation effects on shear localization in porous plastic solids. International Journal of Fracture 19:163-182.

Semiatin S.L. and Jonas J.J., (1984). Formability and Workability of Metals: Plastic Instability and Flow Localization, American Society for Metals, Metals Park.

Tang N.Y., Niessen P. and Pick R.J., (1991). An Investigation of Shock-Induced Damage in Oxygen-free High Conductivity Copper. Materials Science and Engineering A 131:153-160.

Tao G., Chen H. and Shen Q., (2008). Superplastic flow problems of copper shaped-charge jets. Explosion and Shock Waves 28:336-340.

Tvergaard V., (1982). Ductile fracture by cavity nucleation between larger voids. Journal of the Mechanics and Physics of Solids 30(4):265-286.

Weickert C.A. and Gallagher P.J., (1993). Penetration of explosively formed projectiles. International Journal of Impact Engineering 14:809-818.

Weickert C.A. and Gallagher P.J., (1996). Ogive-nosed, finned, explosively-formed projectiles. In: Proceedings of the 16th international symposium on ballistics. San Francisco, California: International Ballistics Society:613-614.

Weimann K. and Doenngsfeld K., (1990). Modeling, testing, and analysis of EFP performance as a function of confinement. In: Proceedings of the 12th international symposium on ballistics. San Antonio, Texas: American Defense Preparedness Association:228-237.

Wu J., Liu J.B. and Du Y.X., (2007). Experimental and numerical study on the flight and penetration properties of explosively-formed projectile. International Journal of Impact Engineering 34:1147-1162.

Ye X.S., (2003). Basis of dynamics explosion, Engineering Institute of Engineering Corps. PLA University of Science and Technology, Nanjing:238-245.

Yu C., Tong Y., Yan C., et al, (1999). Applied research of shaped charge technology. International Journal of Impact Engineering 23:981-988.

Zhang Y., Long Y., Ji C., et al, (2012). Superposition effect of shock waves on formation of a grouped multiple explosive formed projectile. Journal of vibration and shock 31:56-60.